IEEE Access
Multidisciplinary : Rapid Review : Open Access Journal

Received April 23, 2020, accepted May 7, 2020, date of publication May 12, 2020, date of current version May 28, 2020.

*Digital Object Identifier 10.1109/ACCESS.2020.2993999*

# A Simple High-Gain Millimeter-Wave Leaky-Wave Slot Antenna Based on a Bent Corrugated SIW

**YUXIN LIN[1,*], YIMING ZHANG[1,*], HUI LIU[1,2,3], (Member, IEEE), YUAN ZHANG[1], ERIK FORSBERG[2], (Member, IEEE), AND SAILING HE[1,2,3,4], (Fellow, IEEE)**

[1]RF Circuit and Microwave System Laboratory, Centre for Optical and Electromagnetic Research, South China Academy of Advanced Optoelectronics, South China Normal University, Guangzhou 510006, China
[2]RF Circuit and Microwave System Laboratory, Centre for Optical and Electromagnetic Research, National Engineering Research Center for Optical Instruments, Zhejiang University, Hangzhou 310058, China
[3]Ningbo Research Institute, Zhejiang University, Ningbo 315100, China
[4]Department of Electromagnetic Engineering, School of Electrical Engineering, KTH Royal Institute of Technology, 100 44 Stockholm, Sweden

Corresponding authors: Hui Liu (liuhuizju@zju.edu.cn) and Sailing He (sailing@kth.se)

*Yuxin Lin and Yiming Zhang contributed equally to this work.

This work was supported in part by the National Natural Science Foundation of China under Grant 61774131 and Grant 11621101, and in part by the National Key Research and Development Program of China under Grant 2018YFC1407500.

**ABSTRACT** We propose a bent corrugated substrate integrated waveguide (BCSIW) structure that can be used to design a high gain leaky wave antenna (LWA). The design removes the need for a metallic via fabrication process needed for standard substrate integrated waveguides (SIW) and displays superior performance to previously reported structures. We use simulations to compare the performance of the proposed BCSIW LWA to equivalent standard SIW and corrugated SIW (CSIW) structures, as well as experimentally characterize a fabricated BCSIW LWA. Simulation results show that the BCSIW structure can help improve the impedance bandwidth of a slotted LWA by about 14.7% while still maintaining high gain (about 13.2-17.4 dBi) as compared to an LWA based on a CSIW structure. Measurement results indicate that the proposed BCSIW LWA has a wide impedance bandwidth (32.6%) and a high peak gain (12-16.2 dBi) throughout a large frequency range from 22 to 29.2 GHz with a large beam angle range from $-69^\circ$ to $-10^\circ$.

**INDEX TERMS** Leaky-wave antenna (LWA), substrate integrated waveguide (SIW), bent corrugated, low-cost.

## I. INTRODUCTION

In 2016, the Federal Communications Commission (FCC) announced the operating frequency spectrum for the development of wireless technology towards fifth generation (5G) technology, which included the millimeter-wave (mmW) operating band 27.5-28.35 GHz for 5G communication [1]. The International Telecommunication Union (ITU) has similarly identified the band from 24.25-27.5 GHz for 5G communication [2]. However, currently available millimeter-wave devices are in general not commercially viable because of severe attenuation and limitations due to e.g. line-of-sight issues. Thus, there is a need for antennas that have a low profile, low cost, a compact structure and high gain to enable effective 5G communication devices and wireless networks [3]. This has in recent years promoted a large amount of work aimed at rapid development of planar leaky-wave antennas (LWAs) based on various types of radiation structures [4]–[6]. Among these planar LWAs, substrate integrated waveguide (SIW) has attracted much interest due to advantages such as low loss, easy fabrication and cost-effectiveness [7]–[10].

SIW-based planar one-dimensional (1D) LWAs can be classified into two groups: uniform (or quasi-uniform) and periodic. Uniform LWAs have a periodic radiator structure with a period much smaller than the guided wavelength and in which the guided wave is a fast-wave with respect to the free space. The phase constant is smaller than in free space, meaning that these fast-wave LWAs are able to radiate directly. An example from the literature of uniform LWA devices is a half-mode substrate integrated waveguide leaky-wave antenna (HWSIW-LWA) with wide impedance bandwidth and a quasi-omnidirectional radiation pattern [11]. By etching straight long slots, periodic transverse slots and

The associate editor coordinating the review of this manuscript and approving it for publication was Weiren Zhu.

periodic H-shaped slots on the top of uniform SIW structures it is possible to achieve low sidelobe levels, wide impedance bandwidth as well as narrow beams and circular polarization [12]–[14]. Periodic LWAs have a radiator structure with a period that is comparable to the wavelength of the guided wave and thus periodic LWAs typically support a non-radiating fundamental mode (a slow-wave with respect to the free space) while the first-harmonic mode is in the fast-wave region, i.e. periodic LWAs radiate from the first-harmonic mode. Periodic $-45°$ slots, periodic antipodal tapered slots and T-shaped transverse and longitudinal slots etched on the top of periodic SIW structures have been shown to being able to produce effects such as linear and circular polarization as well as broadside scanning performance [15]–[17].

To replace metallic vias while maintaining the advantages of the SIW, Chen *et al.* proposed a corrugated SIW (CSIW) structure, which uses open-circuit quarter wavelength microstrip stubs in lieu of metallic vias in order to artificially create electric sidewalls [18]. Such a structure supports the $TE_{10}$ mode in the same manner as an SIW structure does [19]. In comparison with an SIW structure, the CSIW maintains the DC isolation between the top and bottom conductors by use of the open-circuit quarter wavelength stubs instead of metallic vias. CSIW structure enables tunable leaky-wave antennas, and a beam scanning antenna using an electronically controlled LWA based on a CSIW was recently proposed [20]. In order to reduce the length of the quarter-wavelength open-stubs, a half-mode CSIW structure utilizing bent (or fan-shaped) quarter-wavelength open-stubs was recently proposed [21], however, the design suffers from drawbacks such as small scanning angle range, complex structure and fabrication, as well as low gain.

In this paper we introduce an LWA based on a whole-mode bent corrugated SIW (BCSIW) with periodic transverse slots. We analytically compare the performance of our proposed structure with equivalent SIW and CSIW LWAs, and we experimentally analyze a fabricated BCSIW LWA. The use of bent open-circuit quarter wavelength stubs results in a wider impedance bandwidth while maintaining high gain and low sidelobe levels as compared to SIW and CSIW LWAs.

## II. DESIGN AND COMPARISON OF SIW, CSIW AND BCSIW LWAs

As discussed in the introduction, unlike a conventional SIW structure, a CSIW structure creates electrical sidewalls using open-circuit quarter-wavelength microstrip stubs in lieu of metallic vias in the SIW structure. Utilizing bent microstrip stubs will further increase the performance as as will be shown in the following. Equivalent SIW, CSIW and BCSIW structures are shown in Fig. 1(a)-(c), respectively, and corresponding simulated electrical field distributions at 25 GHz are shown in Fig. 1(d)-(f), where it can be clearly seen that all structures support the same $TE_{10}$ mode. It is thus feasible to design periodic BCSIW LWAs utilizing the same theoretical basis as for periodic SIW LWAs.

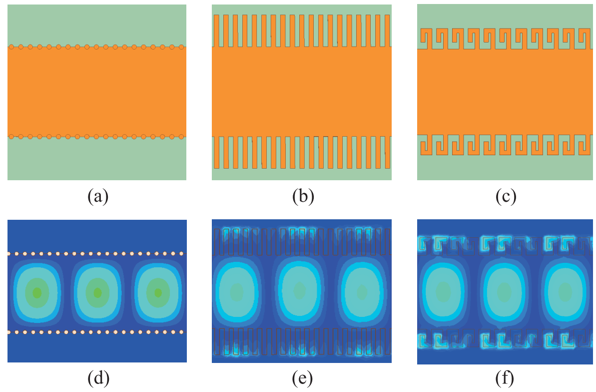


**FIGURE 1.** Structural design (a-c) and electrical field distributions at 25 GHz (d-f) of SIW, CSIW and BCSIWs with equivalent waveguide widths.

As indicated in Fig. 1 (c), the bent open-circuit quarter wavelength stubs can be divided into three parts with lengths $L_1$, $L_2$ and $L_3$. The total length, $L_1 + L_2 + L_3$, should be about one quarter of the guided wavelength. The specific lengths of $L_1$, $L_2$ and $L_3$ through simulation by minimizing the return loss and insertion loss of the BCSIW. Fig. 2(a)-(f) show the return loss and insertion loss of BCSIW at different $L_1$, $L_2$ and $L_3$. From Fig. 2, we see that $S_{11}$ changes partly with different $L_1$, $L_2$ and $L_3$ in the band 21-24 GHz and increases slightly with increasing $L_1$, $L_2$ and $L_3$ in the band 24-30 GHz, while $S_{21}$ decreases in the band 21-26 GHz and increases in the band 26-30 GHz with decreasing $L_1$, $L_2$ and $L_3$. Based on these simulation results, the optimized values ($L_1 = 1.8$ mm, $L_2 = 1.0$ mm, $L_3 = 1.2$ mm) are chosen.

As an example of a simple and effective radiator, rectangular slots are etched on the upper surface of the waveguide [22] to enable the LWA radiate. The required slot length can be estimated by

$$l = \frac{\lambda_0}{4\sqrt{\varepsilon_r}}. \tag{1}$$

where $\lambda_0$ is the wavelength at the operating center frequency in free space, and $\varepsilon_r$ is relative permittivity of the antenna substrate [23]. We choose, in accordance with [23], the slot width, $w$, to satisfy $w/l \ll 1$.

For a uniform LWA, the phase constant, $\beta$, is smaller than the wavenumber in the free space $k_0$, and the radiation angle $\theta$ is defined by

$$\sin\theta = \beta/k_0. \tag{2}$$

However, for a periodic LWA, $\beta$ is larger than $k_0$ and thus a periodic LWA should be designed to allow the first space harmonic ($n = -1$) to radiate instead of the fundamental harmonic, i.e. the radiation angle is defined by

$$\sin\theta = \beta_{-1}/k_0. \tag{3}$$

where $\beta_{-1}$ is the phase constant of the $n = -1$ space harmonic. The phase constant of the $n$th space harmonic is defined as

$$\beta_n = \beta + \frac{2n\pi}{p}. \tag{4}$$

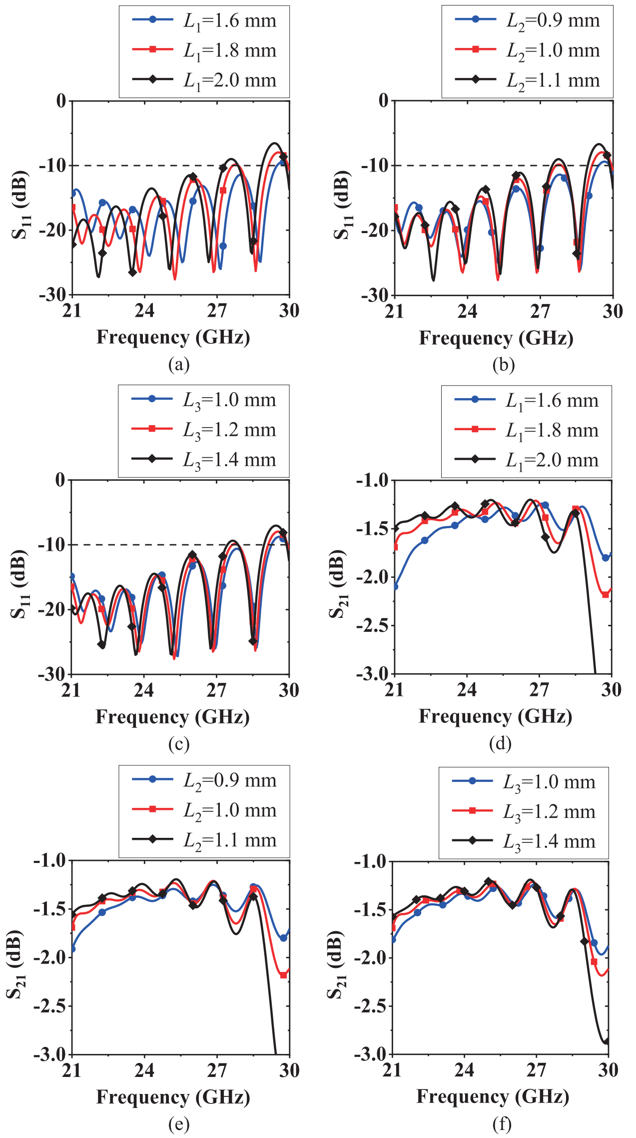


**FIGURE 2.** **Optimization of $L_1$, $L_2$ and $L_3$ through minimization of $S_{11}$ and $S_{21}$. (a-c) Simulated $S_{11}$ with at varying $L_1$, $L_2$ and $L_3$, respectively. (d-f) Simulated $S_{21}$ at varying $L_1$, $L_2$ and $L_3$, respectively.**

where $p$ is the period of the structure. In the first space harmonic mode, the periodic LWA can radiate in either the forward direction or the backward direction.

In the below we optimize the design of SIW, CSIW and BCSIW LWAs through numerical simulations. ANSYS HFSS 18.0 simulation software is used throughout.

The overall geometry of the periodic BCSIW LWA is depicted in Fig. 3(a). Taconic TLY-5-0200 for the substrate; it has a thickness of $h = 0.51$ mm, a dielectric constant of $\varepsilon_r = 2.2$ and a loss tangent of $\tan\sigma = 0.0009$. $L \times W$ are the total dimensions of the BCSIW LWA and $P_{slot}$ is the period of the slots. Plastic screws with diameter $D_v$, placed a distance $P_v$ apart, are used to fix the LWA. Fig. 3(b) details a microstrip taper, which is designed for the antenna feeding line. The use of a tapered microstrip enables the BCSIW waveguide to a 2.92 mm end-launcher with better impedance

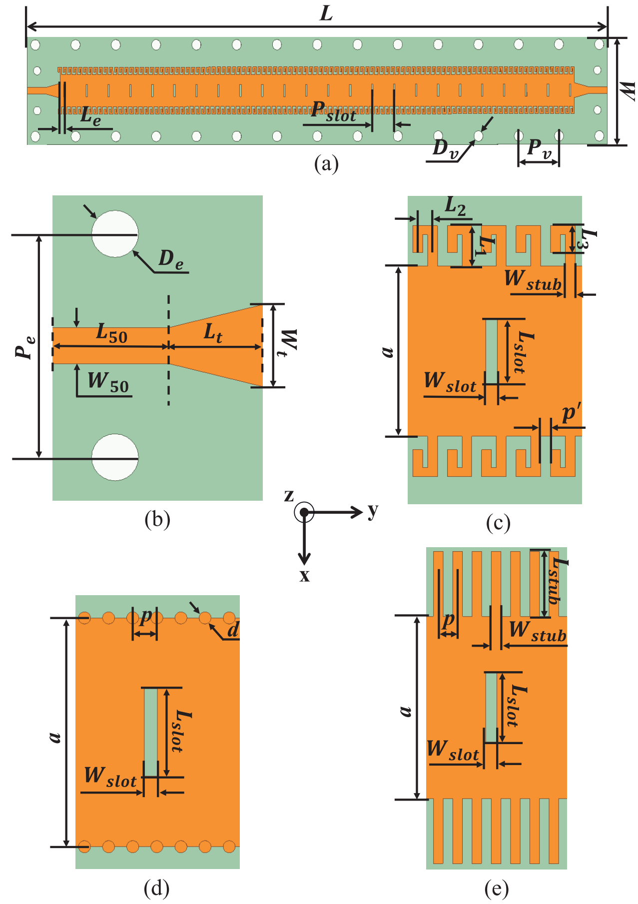


**FIGURE 3.** **(a) BCSIW LWA full structure. (b) Enlarged view of the microstrip taper structure designed for improved coupling to the BCSIW LWA. (c)-(e) Unit cell of the BCSIW LWA, SIW LWA and CSIW LWA, respectively.**

matching for the antenna input port as compared to a traditional strip line. $D_e$ is the diameter of the assembly holes for the 2.92 mm end-launcher and $P_e$ is the distance between the two assembly holes at either side of the end-launcher. $L_{50} \times W_{50}$ are the dimensions of the 50 Ω microstrip feeding line. $L_t$ is the length of the tapered structure and $W_t$ is the width of the wide side of the tapered structure. Fig. 3(c) shows detailed notations for a unit cell of the BCSIW LWA. The dimensions of the slot are $L_{slot} \times W_{slot}$. The width of the waveguides is $a$. All the stubs have the same width $W_{stub}$, and $p'$ is the gap distance between the short part of one bent stub and the long part of an adjacent bent stub.

We compare the performance of the BCSIW LWA with equivalent designs of SIW and CSIW LWAs, the unit cells of which are depicted in Fig. 3(d) and (e). The tapered microstrip structure for the coupling to the SIW and CSIW LWAs is the same as for the BCSIW LWA. The diameter of the metallic vias $d$ and the period of metallic vias $p$ are designed according to SIW theory [8]. The length and width of the CSIW LWA microstrip stubs are $L_{stub} \times W_{stub}$. For the SIW and CSIW LWAs, the dimensions and the period of the slots are kept the same as for the BCSIW LWA for objective comparison of the radiation characteristics of the three structures. We note that

**TABLE 1.** Geometry parameters for the SIW, CSIW and BCSIW LWAs.

| Symbol | SIW LWA | CSIW LWA | BCSIW LWA |
|---|---|---|---|
| $L$ | 158.4 mm | | |
| $W$ | 19.6 mm | 25 mm | 22.4 mm |
| $L_{slot}$ | 2.9 mm | | |
| $W_{slot}$ | 0.45 mm | | |
| $P_{slot}$ | 6 mm | | |
| $a$ | 7.6 mm | | |
| $D_e$ | 2 mm | | |
| $P_e$ | 9.5 mm | | |
| $D_v$ | 2.5 mm | | |
| $P_v$ | 11 mm | | |
| $L_{50}$ | 5 mm | | |
| $W_{50}$ | 1.54 mm | | |
| $L_t$ | 4 mm | | |
| $W_t$ | 3.4 mm | | |
| $L_e$ | 0.975 mm | | |
| $d$ | 0.4 mm | | |
| $p$ | 0.8 mm | 0.8 mm | |
| $L_{stub}$ | | 2.7 mm | |
| $W_{stub}$ | | 0.4 mm | 0.4 mm |
| $L_1$ | | | 1.8 mm |
| $L_2$ | | | 1 mm |
| $L_3$ | | | 1.2 mm |
| $p'$ | | | 0.4 mm |

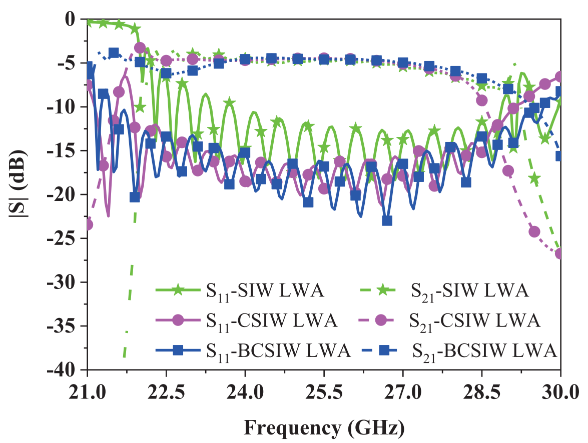


**FIGURE 4.** Simulated S-parameters for the SIW, CSIW and BCSIW LWAs.

the period $p$ of the SIW metallic vias and the period of CSIW microstrip stubs are the same. We summarize the parameters of the SIW, CSIW and BCSIW LWAs in Table 1.

Simulated $S$-parameters of the SIW, CSIW and BCSIW LWAs are shown in Fig. 4, where it can be seen that $S_{11}$ is below $-10$ dB from 21.45 to 29.65 GHz for the BCSIW LWA while from 23.8 to 28.85 GHz for the SIW LWA and from 21.95 to 29.1 GHz for the CSIW LWA; i.e. the $-10$ dB impedance bandwidth of the BCSIW LWA is 62.3% larger than that of the SIW LWA and is 14.7% larger than that of the CSIW LWA. $S_{21}$ is lower than $-4.0$ dB in the impedance band (defined as the frequency range where $S_{11}$ is below $-10$ dB) for the BCSIW LWA while lower than $-4.4$ dB for the SIW LWA and lower than $-3.3$ dB for the CSIW LWA. Fig. 5 shows the simulated realized gain of the SIW, CSIW and BCSIW LWAs at various frequencies in the BCSIW LWA impedance band. We note that the realized gain of the SIW LWA is $-3.33$ dBi at 22 GHz, i.e. the SIW LWA cannot radiate effectively at 22 GHz. We furthermore notice that the realized gain of the BCSIW LWA on average is higher than that of the SIW LWA and CSIW LWA in the BCSIW LWA impedance band. Fig. 6 shows simulated normalized radiation patterns of the co-polarized fields in the $yz$-plane of the SIW, CSIW and BCSIW LWAs at 22, 23.2, 24.4, 25.6, 26.8, 28 and 29.2 GHz. The sidelobe level of the three LWAs are overall similar, however it is better for the BCSIW LWA than for the SIW and CSIW LWAs at 22 GHz. Though all three LWAs have the same size fixed radiating elements, the radiation beam angle of the SIW LWA is somewhat tilted compared with those of the CSIW and BCSIW LWA, which is due to the microstrip stubs. Due to the bent microstrip stubs, the impedance bandwidth of BCSIW LWA is larger than those for the other two LWAs, and consequently the total scan angle within the impedance bandwidth of the BCSIW LWA is larger than for the other two LWAs. Within the respective impedance bandwidth of the three antennas, the total scan angles are found to be: BCSIW LWA: $-69°$ to $-10°$ (impendence bandwidth 22-29.2 GHz); SIW LWA: $-46°$ to $-21°$ ( impendence bandwidth: 24.4-28 GHz); and CSIW LWA: $-67°$ to $-17°$ (impendence bandwidth: 22-28 GHz).

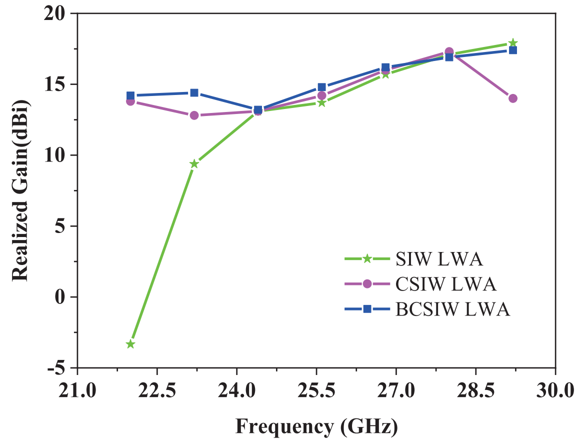


**FIGURE 5.** Simulated realized gain for the SIW, CSIW and BCSIW LWAs.

Table 2 compares the impedance bandwidths of the three LWAs. Each frequency point where $S_{11}$ is below $-10$ dB, is ticked. The scan angles corresponding to the $-10$ dB impedance bandwidths are shown in the last row and we can see that the BCSIW LWA has both the largest bandwidth and the largest scan angle.

## III. EXPERIMENTAL CHARACTERIZATION OF THE BCSIW LWA AND COMPARISON WITH SIMULATIONS

The proposed BCSIW LWA was fabricated (as shown in Fig. 7) and measured for verification. The two ports of the BCSIW LWA are connected by two end launch connectors,

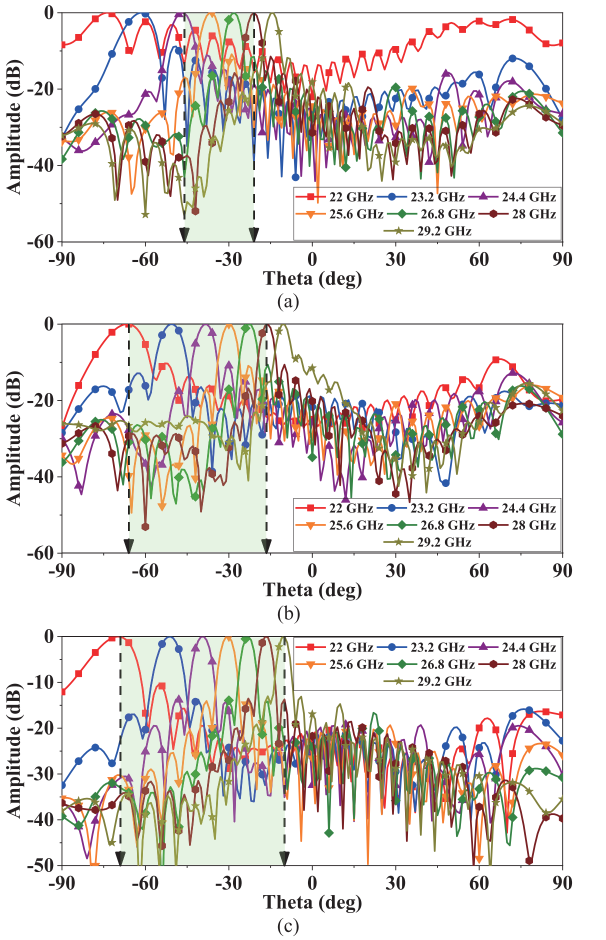


**FIGURE 6.** Simulated normalized radiation patterns of co-polarized fields in the *yz*-plane at 22, 23.2, 24.4, 25.6, 26.8, 28 and 29.2 GHz for the SIW (a), CSIW (b) and BCSIW LWAs (c).

**TABLE 2.** Impedance bandwidth performance summary of the three LWAs. Frequency points where $S_{11}$ is below −10 dB are ticked. The corresponding scan angles are shown in the last row.

| | SIW LWA | CSIW LWA | BCSIW LWA |
|---|---|---|---|
| 22 GHz | | √ | √ |
| 23.2 GHz | | √ | √ |
| 24.4 GHz | √ | √ | √ |
| 25.6 GHz | √ | √ | √ |
| 26.8 GHz | √ | √ | √ |
| 28 GHz | √ | √ | √ |
| 29.2 GHz | | | √ |
| Scan Angles | 25° | 50° | 59° |

and $S_{11}$ was measured using an Agilent N5247A network analyzer. Measured $S$-parameters are shown in Fig. 8 together with the previously simulated values, both of which is less than −10 dB in the band of interest (i.e. from 22 to 29.2 GHz). The measured impedance bandwidth 21.3 - 29.6 GHz is slightly wider than the simulated result (21.45 - 29.65 GHz), which we attribute due to fabrication error. Both the measured and simulated results show that $S_{11}$ is less than −10 dB in the band of interest (i.e. from 22 to 29.2 GHz). The measured $S_{21}$ is in the range −7.1 to −22.0 dB, which is lower than the simulated $S_{21}$ (−4.0 to −15.6 dB). The discrepancy between the simulated and measured $S_{21}$, can, in parts, as well be attributed to fabrication error, however also due to loss in two adaptors, which have an insertion loss of $0.05 \times \sqrt{f(GHz)}$ (dB), that are used to connect the BCSIW LWA to the two ports of the network analyzer.

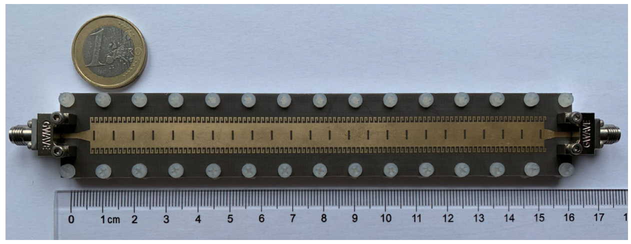

**FIGURE 7.** Fabricated BCSIW LWA prototype.

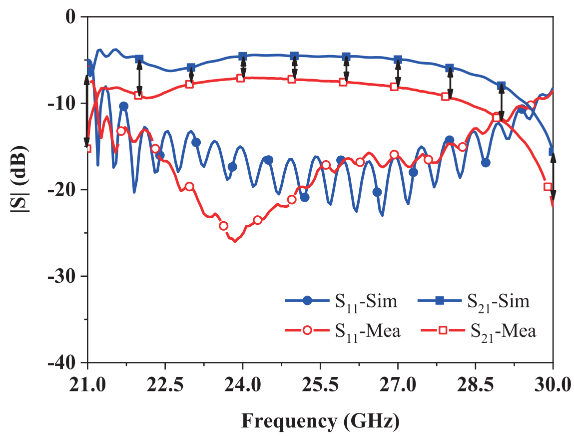


**FIGURE 8.** Simulated and measured *S*-parameters of the BCSIW LWA.

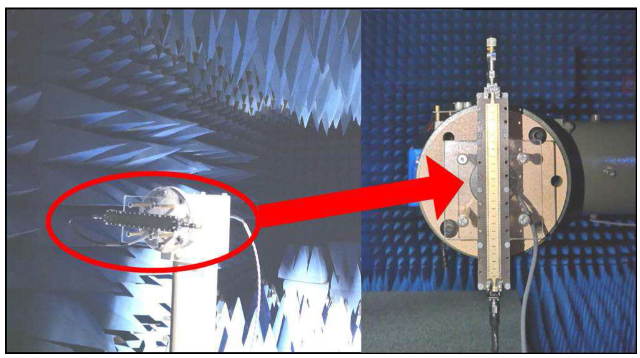

**FIGURE 9.** Setup for measuring the gain of the BCSIW LWA in an anechoic chamber test.

Fig. 9 shows the setup of the microwave anechoic chamber test, in which one port of the antenna is terminated by a 50 Ω load for the gain measurement. Fig. 10 shows the simulated and measured realized gains of the BCSIW LWA at different frequencies. The measured realized gain agrees well with the simulated result with a variation of less than 2.3 dBi, which is attributed to losses in the coaxial waveguide and

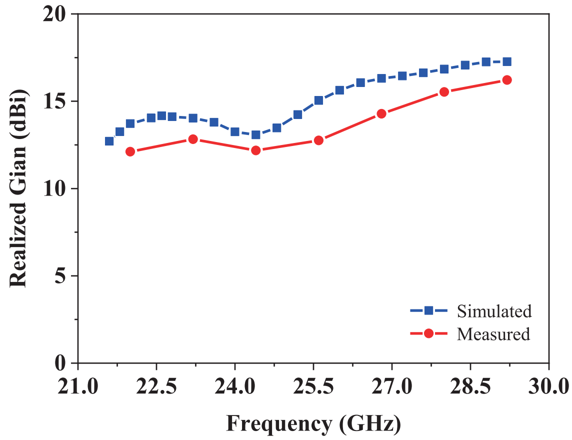


**FIGURE 10.** Simulated and measured realized gains for the BCSIW LWA.

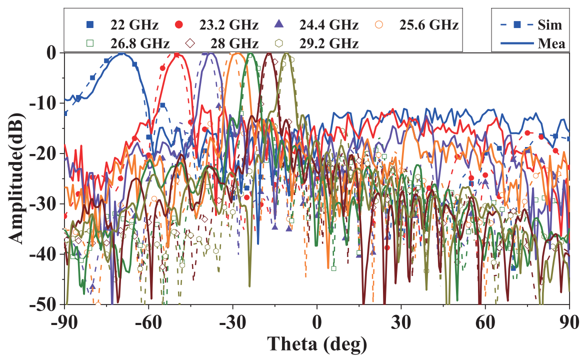


**FIGURE 11.** Simulated and measured normalized radiation patterns of the co-polarized fields for the BCSIW LWA at 22, 23.2, 24.4, 25.6, 26.8, 28 and 29.2 GHz.

fabrication error. In the range 22 - 29.2 GHz, the maximum realized gain is 16.2 dBi at 29.2 GHz. Simulated and measured normalized radiation patterns of the co-polarized fields are illustrated in Fig. 11. The measured normalized radiation patterns show that the scan angle of the fabricated BCSIW LWA can be swept from −69° to −10° when the frequency is scanned from 22 to 29.2 GHz, which again agree well with the simulated results. Furthermore, the sidelobe levels of the measured radiation patterns at chosen frequencies are all below −10 dB. Although there is a shift between the measured and simulated sidelobe level due to cable losses and fabrication errors, the measured and simulated curves overall agree well with each other. Use of better adaptors and connectors with lower loss, and higher precision fabrication are expected to improve the results.

## IV. COMPARISON WITH PREVIOUS WORK

In Table 3 we compare the pertinent parameters and performance between our proposed BCSIW LWA and previously published LWAs and we can see that the bandwidth, scanning range and the measured gain of the BCSIW LWA are better than those in Refs [13], [24], [25] and [27]. Comparing to the SIGW LWA in Ref [26], the measured bandwidth, scanning range and length (compactness) of the BCSIW LWA are much better, though the measured gain is slightly smaller.

**TABLE 3.** Comparison of the proposed BCSIW LWA with previously published LWAs.

| Antenna | Center frequency (GHz) | BW (%) | Gain (dBi) | Dimensions ($\lambda_0$) | Scanning Range |
|---|---|---|---|---|---|
| SIW LWA [13] | 11.10 | 22 | 12 | 12 × 0.48 × 0.04 | 50° |
| MED LWA [24] | 30.15 | 20 | 15.6 | 12 × 1.4 × 0.24 | 16° |
| SIW LWA array [25] | 14.75 | 10 | 7 | 9 × 1.48 × 0.08 | 13° |
| SIGW LWA [26] | 58.50 | 27 | 17.7 | 28 × - × 0.15 | 20° |
| Printed LWA [27] | 23.50 | 4 | 14.9 | - | 9° |
| BCSIW LWA | 25.45 | 33 | 16.2 | 13 × 1.9 × 0.04 | 59° |

## V. CONCLUSION

In this paper, a BCSIW LWA for millimeter-wave applications has been proposed and compared with equivalent SIW and CSIW LWAs using simulations. Here the specific shape is just as a simple and natural example to illustrate the principle how bent stubs in CSIW can improve the performance of an LWA.The BCSIW LWA is also fabricated and characterized. The measured impedance bandwidth reaches 32.6% around the center frequency of 25.45 GHz with a measured peak gain of 16.2 dBi at 29.2 GHz and a smaller than −10 dB sidelobe level. Furthermore, the scan angle ranges from −69° to −10° when the frequency is scanned from 22 to 29.2 GHz. By bending the open-circuit quarter wavelength stubs of an equivalent whole-mode CSIW LWA, the total width of the BCSIW LWA is reduced by about 10.4%. Compared to the equivalent CSIW LWA, the BCSIW LWA impedance bandwidth ($S_{11}$ below −10 dB) is about 14.7% larger. Good agreement between the simulated and measured results of the BCSIW LWA has been demonstrated. Having the advantages of easy fabrication, wide impedance bandwidth and high gain, the BCSIW LWA proposed in this paper has strong potential for use in 5G communication applications.

## ACKNOWLEDGMENT

The authors would like to thank Prof. X. Wu and Prof. J. Zhou from the College of Information Science and Electronic Engineering at Zhejiang University, as well as Dr. B. Wei at the Training Platform of Information and Microelectronic Engineering at the Polytechnic Institute of Zhejiang University, for their help in antenna performance measurement.

## REFERENCES

[1] FCC. (2016). *Use of Spectrum Bands Above 24 GHz For Mobile Radio Services*, Accessed: Oct. 1, 2019. [Online]. Available: https://www.fcc.gov/document/spectrum-frontiers-ro-and-fnprm

[2] ITU-R. (2018). *Adjacent Band Compater Study Between IMT-2020 24.25-27.5 GHz EESS 23.6-24 GHz*. Accessed: Dec. 1, 2019. [Online]. Available: https://www.itu.int/md/R15-TG5.1-C-0350/en

[3] W. Cao, W. Hong, Z. N. Chen, B. Zhang, and A. Liu, "Gain enhancement of beam scanning substrate integrated waveguide slot array antennas using a phase-correcting grating cover," *IEEE Trans. Antennas Propag.*, vol. 62, no. 9, pp. 4584–4591, Sep. 2014.

[4] Q. Zhang, Q. Zhang, and Y. Chen, "Spoof surface plasmon polariton leaky-wave antennas using periodically loaded patches above PEC and AMC ground planes," *IEEE Antennas Wireless Propag. Lett.*, vol. 16, pp. 3014–3017, Oct. 2017.

[5] W. Ma, W. Cao, S. Shi, Z. Zeng, and X. Yang, "Gain enhancement for circularly polarized SIW frequency beam scanning antenna using a phase-correcting grating cover," *IEEE Access*, vol. 7, pp. 52680–52688, 2019.

[6] J. Zhang, X. Ge, Q. Li, M. Guizani, and Y. Zhang, "5G millimeter-wave antenna array: Design and challenges," *IEEE Wireless Commun.*, vol. 24, no. 2, pp. 106–112, Apr. 2017.

[7] M. Bozzi, A. Georgiadis, and K. Wu, "Review of substrate integrated waveguide (SIW) circuits and antennas," *IET Microw., Antennas Propag.*, vol. 5, no. 8, pp. 909–920, Jun. 2011.

[8] E. Massoni, M. Bozzi, and K. Wu, "Increasing efficiency of leaky-wave antenna by using substrate integrated slab waveguide," *IEEE Antennas Wireless Propag. Lett.*, vol. 18, no. 8, pp. 1596–1600, Aug. 2019.

[9] Y.-L. Lyu, F.-Y. Meng, G.-H. Yang, D. Erni, Q. Wu, and K. Wu, "Periodic SIW leaky-wave antenna with large circularly polarized beam scanning range," *IEEE Antennas Wireless Propag. Lett.*, vol. 16, pp. 2493–2496, 2017.

[10] F. Xu and K. Wu, "Guided-wave and leakage characteristics of substrate integrated waveguide," *IEEE Trans. Microw. Theory Techn.*, vol. 53, no. 1, pp. 66–73, Jan. 2005.

[11] J. Xu, W. Hong, H. Tang, Z. Kuai, and K. Wu, "Half-mode substrate integrated waveguide (HMSIW) leaky-wave antenna for millimeter-wave applications," *IEEE Antennas Wireless Propag. Lett.*, vol. 7, pp. 85–88, Apr. 2008.

[12] Y. J. Cheng, W. Hong, K. Wu, and Y. Fan, "Millimeter-wave substrate integrated waveguide long slot leaky-wave antennas and two-dimensional multibeam applications," *IEEE Trans. Antennas Propag.*, vol. 59, no. 1, pp. 40–47, Jan. 2011.

[13] J. Liu, D. R. Jackson, and Y. Long, "Substrate integrated waveguide (SIW) leaky-wave antenna with transverse slots," *IEEE Trans. Antennas Propag.*, vol. 60, no. 1, pp. 20–29, Jan. 2012.

[14] J. Liu, X. Tang, Y. Li, and Y. Long, "Substrate integrated waveguide leaky-wave antenna with H-Shaped slots," *IEEE Trans. Antennas Propag.*, vol. 60, no. 8, pp. 3962–3967, Aug. 2012.

[15] Y. Jian Cheng, W. Hong, and K. Wu, "Millimeter-wave half mode substrate integrated waveguide frequency scanning antenna with quadri-polarization," *IEEE Trans. Antennas Propag.*, vol. 58, no. 6, pp. 1848–1855, Jun. 2010.

[16] R. Henry and M. Okoniewski, "A broadside scanning substrate integrated waveguide periodic phase-reversal leaky-wave antenna," *IEEE Antennas Wireless Propag. Lett.*, vol. 15, pp. 602–605, 2016.

[17] Y.-L. Lyu, X.-X. Liu, P.-Y. Wang, D. Erni, Q. Wu, C. Wang, N.-Y. Kim, and F.-Y. Meng, "Leaky-wave antennas based on noncutoff substrate integrated waveguide supporting beam scanning from backward to forward," *IEEE Trans. Antennas Propag.*, vol. 64, no. 6, pp. 2155–2164, Jun. 2016.

[18] D. G. Chen and K. W. Eccleston, "Substrate integrated waveguide with corrugated wall," in *Proc. Asia–Pacific Microw. Conf.*, Dec. 2008, pp. 1–4.

[19] K. W. Eccleston, "Corrugated substrate integrated waveguide distributed amplifier," in *Proc. Asia Pacific Microw. Conf. Process.*, Dec. 2012, pp. 379–381.

[20] K. Chen, Y. H. Zhang, S. Y. He, H. T. Chen, and G. Q. Zhu, "An electronically controlled leaky-wave antenna based on corrugated SIW structure with fixed-frequency beam scanning," *IEEE Antennas Wireless Propag. Lett.*, vol. 18, no. 3, pp. 551–555, Mar. 2019.

[21] T. Lou, X.-X. Yang, H. Qiu, Q. Luo, and S. Gao, "Low-cost electrical beam-scanning leaky-wave antenna based on bent corrugated substrate integrated waveguide," *IEEE Antennas Wireless Propag. Lett.*, vol. 18, no. 2, pp. 353–357, Feb. 2019.

[22] J. Liu, W. Zhou, and Y. Long, "A simple technique for open-stopband suppression in periodic leaky-wave antennas using two nonidentical elements per unit cell," *IEEE Trans. Antennas Propag.*, vol. 66, no. 6, pp. 2741–2751, Jun. 2018.

[23] Y. Mohtashami and J. Rashed-Mohassel, "A butterfly substrate integrated waveguide leaky-wave antenna," *IEEE Trans. Antennas Propag.*, vol. 62, no. 6, pp. 3384–3388, Jun. 2014.

[24] K.-M. Mak, K.-K. So, H.-W. Lai, and K.-M. Luk, "A magnetoelectric dipole leaky-wave antenna for millimeter-wave application," *IEEE Trans. Antennas Propag.*, vol. 65, no. 12, pp. 6395–6402, Dec. 2017.

[25] Y. Geng, J. Wang, Z. Li, Y. Li, M. Chen, and Z. Zhang, "A leaky-wave antenna array with beam-formed radiation pattern for application in a confined space," *IEEE Access*, vol. 7, pp. 86367–86373, 2019.

[26] M. R. Rahimi, N. Bayat-Makou, and A. A. Kishk, "Millimeter-wave substrate integrated gap waveguide leaky-wave antenna for WiGig applications," *IEEE Trans. Antennas Propag.*, vol. 67, no. 9, pp. 5790–5800, Sep. 2019.

[27] M. V. Kuznetcov, V. G.-G. Buendia, Z. Shafiq, L. Matekovits, D. E. Anagnostou, and S. K. Podilchak, "Printed leaky-wave antenna with aperture control using width-modulated microstrip lines and TM surface-wave feeding by SIW technology," *IEEE Antennas Wireless Propag. Lett.*, vol. 18, no. 9, pp. 1809–1813, Sep. 2019.

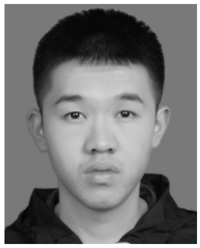

**YUXIN LIN** was born in Foshan, China. He received the B.S degree in physics from South China Normal University, China, in 2018, where he is currently pursuing the M.S. degree in electrical engineering. His current research interests include leaky-wave antennas and arrays.

**YIMING ZHANG** received the B.S. degree in electronic science and technology from the Shaanxi University of Science and Technology, Xi'an, China, in 2016. He is currently pursuing the M.S. degree in electromagnetic field and microwave technology from the Centre for Optical and Electromagnetic Research, South China Academy of Advanced Optoelectronics, South China Normal University, Guangzhou, China. His current research interests include RF circuits, RFID antennas, mm-wave antennas, and microwave components.

**HUI LIU** (Member, IEEE) was born in Zhumadian, China. He received the M.S. degree in electromagnetic field and microwave technology from South China Normal University, China, in 2013, and the Ph.D. degree in microelectronics and solid state electronics from the Centre for Optical and Electromagnetic Research, Academy of Advanced Optoelectronics, South China Normal University, in 2018. He is currently a Postdoctoral Researcher with the Center for Optical and Electromagnetic Research, Zhejiang University. His research interests include antenna, RF circuits, and microwave components.

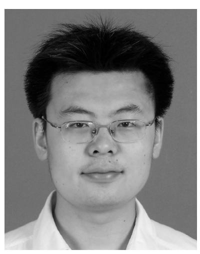

**YUAN ZHANG** was born in Shanxi, China, in 1980. He received the bachelor's and Ph.D. degrees in optical engineering from the Beijing Institute of Technology, Beijing, China, in 2003 and 2009, respectively. Since then, he moved to Nanyang Technological University, Singapore, in 2009, and Zhejiang University, Zhejiang, China, in 2010, as a Postdoctoral Fellow. Since 2014, he has been a Faculty Member of the Centre for Optical and Electromagnetic Research, South China Normal University, Guangzhou, China. His research focuses on metamaterials, artificial electromagnetic structures with interesting properties.

**ERIK FORSBERG** (Member, IEEE) received the M.S. degree in engineering physics and the Ph.D. degree in photonics from the Royal Institute of Technology (KTH), Sweden, in 1996 and 2003, respectively. He also studied business and economics at the Stockholm School of Economics, Sweden. In 2000, he was a Visiting Scientist with Hokkaido University, Japan, and a Postdoctoral Fellow with KTH, in 2003. He was a Faculty Member with Zhejiang University (ZJU), China, from 2004 to 2008. From 2009 until 2012, he was the Founding Graduate Dean (associate) with the Higher Colleges of Technology (HCT), United Arab Emirates. In 2013, he rejoined ZJU as an Associate Professor. His current research interests include nano-lasers, plasmonics and optical fiber devices.

**SAILING HE** (Fellow, IEEE) received the Licentiate and Ph.D. degrees in electromagnetic theory from the Royal Institute of Technology, Stockholm, Sweden, in 1991 and 1992, respectively. He has been with the Department of Electromagnetic Engineering, Royal Institute of Technology, as an Assistant Professor, an Associate Professor, and a Full Professor. He is currently a Professor with the Centre for Optical and Electromagnetic Research, Zhejiang University, China. He has first-authored one monograph (Oxford University Press) and has authored or coauthored more than 600 articles in refereed international journals. He has given many invited/plenary talks in international conferences, and has served in the leadership for many international conferences. His current research interests include electromagnetic metamaterials, optoelectronics, sensing, and communication.